Article

Understanding the Role of Mean and Eddy Momentum Transport in the Rapid Intensification of Hurricane Irma (2017) and Hurricane Michael (2018)

Alrick Green [1], Sundararaman G. Gopalakrishnan [2], Ghassan J. Alaka, Jr. [2] and Sen Chiao [3,*]

[1] Atmospheric Physics, University of Maryland, Baltimore County, Baltimore, MD 21250, USA; agreen15@umbc.edu
[2] Hurricane Research Division, NOAA/AOML, Miami, FL 33149, USA; sundararaman.g.gopalakrishnan@noaa.gov (S.G.G.); ghassan.alaka@noaa.gov (G.J.A.)
[3] Department of Meteorology and Climate Science, San Jose State University, San Jose, CA 95192, USA
* Correspondence: sen.chiao@sjsu.edu; Tel.: +1-408-924-5204

Abstract: The prediction of rapid intensification (RI) in tropical cyclones (TCs) is a challenging problem. In this study, the RI process and factors contributing to it are compared for two TCs: an axis-symmetric case (Hurricane Irma, 2017) and an asymmetric case (Hurricane Michael, 2018). Both Irma and Michael became major hurricanes that made significant impacts in the United States. The Hurricane Weather Research and Forecasting (HWRF) Model was used to examine the connection between RI with forcing from the large-scale environment and the subsequent evolution of TC structure and convection. The observed large-scale environment was reasonably reproduced by HWRF forecasts. Hurricane Irma rapidly intensified in an environment with weak-to-moderate vertical wind shear (VWS), typically favorable for RI, leading to the symmetric development of vortical convective clouds in the cyclonic, vorticity-rich environment. Conversely, Hurricane Michael rapidly intensified in an environment of strong VWS, typically unfavorable for RI, leading to major asymmetries in the development of vortical convective clouds. The tangential wind momentum budget was analyzed for these two hurricanes to identify similarities and differences in the pathways to RI. Results suggest that eddy transport terms associated with convective processes positively contributed to vortex spin up in the early stages of RI and inhibited spin up in the later stages of RI in both TCs. In the early stages of RI, the mean transport terms exhibited notable differences in these TCs; they dominated the spin-up process in Irma and were of secondary importance to the spin-up process in Michael. Favorable aspects of the environment surrounding Michael appeared to aid in the RI process despite hostile VWS.

Keywords: eddy vorticity fluxes; momentum budget; hurricanes rapid intensification; HWRF

1. Introduction

A tropical cyclone (TC) is one of the most dangerous forms of natural disaster to impact society and coastal communities annually. To offer as much preparation time as possible, it is essential to accurately predict the track and changes in intensity associated with these weather systems. Although the prediction of TC intensity change has generally improved [1], TC rapid intensification (RI), defined when the maximum wind speed increases by at least 30 kt (15 m s^{-1}) in a 24 h period [2], remains a great forecast challenge [1,2]. Prior studies have shown that TC intensity variability involves multiscale nonlinear interaction of different variables including vertical wind shear (VWS), mid-level moisture, upper ocean temperatures and heat content, cloud microphysics, air–sea interaction, and inner core dynamics and thermodynamics. All these factors are well known to influence TC RI (e.g., [3–9]).

Environmental VWS interactions with the TC vortex have been investigated by using both in situ observations and numerical simulations (e.g., [10–14]). VWS is widely recog-

nized to be anticorrelated with RI (e.g., [2,8]). Several mechanisms have been proposed to explain why TCs usually weaken in the presence of strong VWS, including TC vortex tilting [11], mid-tropospheric ventilation of the TC inner core [12,13], dilution of the upper-tropospheric TC warm core by divergent fluxes [14], and downdrafts that reduce moist entropy in the boundary layer in the TC inner core region [13].

However, the relationship between VWS and TC intensity is complex, and some TCs have been observed to intensify rapidly in the presence of hostile environmental shear (i.e., >15 m s^{-1}) [14–18]. Chen and Gopalakrishnan [7] investigated the RI of Hurricane Earl (2010) in an environment of strong VWS using the operational Hurricane Weather Research and Forecasting (HWRF) system. A great number of aircraft observations in the inner core were used to verify the forecast of Earl, an asymmetric TC that rapidly intensified in a hostile environment. They concluded that the triggering mechanism for RI was the development of an upper-level warm core over the TC surface center. The upper-level warm core developed due to deep convection and subsidence-induced warm air advection in the upshear left region of the TC. This warm air was transported radially inwards from the upshear left region until it was coincident with the TC surface center position [7].

Another TC that experienced RI in hostile shear was Tropical Storm Gabrielle (2001). Gabrielle was impacted by environmental shear of 13 m s^{-1}) when it underwent RI, with the central pressure dropping by 22 hPa within 3 h [15,16]. Despite hostile VWS, the key factor behind Gabrielle's RI was an intense convective cell. This intense convective cell developed in the downshear left quadrant of the TC and moved cyclonically inward to a radius of 17 km within the radius of maximum winds.

Consequently, this convective cell amplified the efficiency for kinetic energy production to spin up the vortex. Rios-Berrios et al. [17] examined the RI of Hurricane Katia (2011) in a sheared environment using the Advanced Hurricane Weather Research and Forecasting (HWRF) model. Despite the presence of strong environmental shear, they found that Katia rapidly intensified due to moistening of the low to middle troposphere to the right of the shear vector.

Leighton et al. [18] used an experimental ensemble of HWRF forecasts to investigate the RI associated with Hurricane Edouard (2014). Although both intensifying and non-intensifying ensemble members had deep convection in the downshear right quadrant of the TC, convection propagated into the upshear region only in intensifying members. A budget analysis of tangential momentum showed that the radial eddy vorticity flux contributed positively to the spin-up process of tangential winds in the middle to upper troposphere and reduced vortex tilt in the RI members. As for the non-intensifying members, negative eddy vorticity flux spun down the tangential winds in the midddle to upper troposphere, and Edouard's vortex never became vertically aligned.

Gopalakrishnan et al. [19] used a high-resolution version of HWRF to understand the role of shear-induced asymmetries on the intensification of Hurricane Earl (2010). Results from their study revealed that eddy radial vorticity fluxes play a significant role in controlling TC intensity changes in sheared storms. In the case of Earl, despite persistent environmental shear and a lack of symmetric convection, a positive eddy vorticity flux in the middle to upper troposphere created by mesoscale convective complexes had a profound influence in accelerating the TC spin-up process. Clearly, while in one case of sheared storm, eddy vorticity fluxes aided spin-up of the TC vortex, in another case, eddy vorticity fluxes have a negative role.

In this study, two hurricanes that underwent RI were investigated to understand better how TCs spin up in different environments. Hurricane Irma (2017) was embedded in an environment of weak VWS and developed as a nearly symmetric storm. Hurricane Michael (2018), on the other hand, developed in an environment of strong VWS with persistent convection initially only in the northern sector.

The following questions are addressed in this study: What are the differences between the modeled large-scale environmental conditions between the two TCs and how do they verify with reality? How does a hurricane intensify in the presence of environmental shear?

What will be the contributions from the mean and eddy terms in the two different storms? We used the HWRF system and Global Forecast System (GFS) analysis to answer these questions. Section 2 provides case descriptions. Section 3 entails a detailed description of the experimental design and methods behind the research along with modeling and postprocessing tools used. The results from observations and HWRF simulations on each tropical cyclone are presented in Section 4. A summary of the key findings and future research are discussed in Section 5.

2. Case Descriptions

Detailed TC reports on Hurricanes Irma (2017) and Michael (2018) were prepared by the National Hurricane Center [20,21]. Nevertheless, a summary of the large-scale perspectives relevant to the current study is provided here.

2.1. Hurricane Irma (2017)

Irma, a long-lived TC, originated from a tropical wave with widespread deep convection that departed off the west coast of Africa on 27 August 2017. The wave organized into Tropical Depression 11 roughly 200 km west–southwest of the Cabo Verde Islands at 0000 UTC on 30 August 2017. Six hours later, the cyclone strengthened to Tropical Storm Irma and maintained a westward trajectory south of a mid-level ridge over the Atlantic Ocean (for reference, the model simulation was started the same day at 1200 UTC when Irma was still a tropical storm). Irma rapidly intensified into a hurricane by 0600 UTC on 31 August. Favorable conditions, including weak VWS, promoted further development of deep convection and intensification. As a result, Irma continued its RI, reaching major hurricane status (i.e., Category 3 on the Saffir–Simpson scale) at 0000 UTC on 01 September.

For the next 72 h, the intensification process halted due to dry air intrusion and eyewall replacement cycles, which disrupted the intensification process and caused minor fluctuations in intensity. Irma turned to the west–southwest after the mid-level ridge to its north strengthened and, consequently, moved over high sea surface temperatures [20].

Irma reached a maximum intensity of 155 kt (~80 m s^{-1}) at 1800 UTC 05 September after the completion of an eyewall replacement cycle, registering as a Category 5 hurricane. By this point, the TC had become extremely organized with a well-developed eye and symmetric deep convection in the eyewall. Irma made its first landfall on the island of Barbuda at roughly 0600 UTC on 06 September and later in the British Virgin Islands at 1600 UTC. Irma continued as a Category 5 hurricane for more than 48 h before making another landfall in The Bahamas as a Category 4 hurricane on 08 September. On 09 September, Irma weakened to a Category 2 hurricane after prolonged interaction with Cuba. Irma then turned to the northwest in response to a low-pressure system, which brought the TC over the Straits of Florida where high sea surface temperatures (SSTs) supported re-intensification into a Category 4 hurricane. Irma continued to turn to the north, making two final landfalls on Cudjoe Key and Marco Island, Florida on 10 September. Irma rapidly decayed as it moved over the Florida Peninsula and ultimately dissipated over the continental United States [20].

2.2. Hurricane Michael (2018)

Michael, a powerful and short-lived TC, originated from a low-pressure system that became embedded in a large cyclonic gyre over the northwestern Caribbean Sea on 6 October 2018 (for reference, the model simulation was started at 1800 UTC on the same day). At 0600 UTC on 7 October 2018, Michael became a tropical depression located 130 nautical miles south of Cozumel, Mexico with a northward trajectory towards the Gulf of Mexico. Michael began an RI period despite hostile atmospheric conditions, including strong VWS. Michael soon became a tropical storm and later a hurricane at 1200 UTC on 8 October despite persistent southwesterly wind shear.

Michael encountered an abrupt hiatus in intensification as it passed west of Cuba, possibly due to dry air intrusion, a cold ocean eddy, and strong VWS. By 9 October, Michael

resumed its RI process and was steered generally northward toward the continental United States by a mid-level ridge and a mid-level shortwave trough over the northwest Gulf of Mexico. Michael rapidly intensified to a Category 5 hurricane just before it made landfall near Mexico Beach, Florida, with maximum winds of 140 kt (72 m s^{-1}) at 1730 UTC on 10 October. After landfall, Michael rapidly decayed as it moved deeper into the continental United States. By 11 October, Michael transitioned into an extratropical cyclone over North Carolina [21].

3. Experimental Design and Methods

3.1. Model Description

The HWRF system was developed jointly by the National Centers for Environmental Prediction (NCEP) in the National Oceanographic and Atmospheric Administration's (NOAA) National Weather Service (NWS) and the Hurricane Research Division in NOAA's Atlantic Oceanographic and Meteorological Laboratory (AOML) as a part of the Hurricane Forecast Improvement Project (HFIP) [22–27]. HWRF utilizes the WRF Nonhydrostatic Mesoscale Model (WRF–NMM) dynamical core to solve governing equations of dynamics and thermodynamics [28]. Hurricanes Irma (2017) and Michael (2018) were simulated using version 4.0 of the operational HWRF system, an ocean-coupled regional model that utilizes moving nested domains to achieve cloud-resolving scales [29]. The atmospheric component of HWRF is coupled to the Message Passing Interface Princeton Ocean Model-Tropical Cyclone (MPIPOM–TC) via the NCEP coupler. The three nested domains in this version of HWRF have horizontal grid spacings of 13.5 km for the outermost domain, 4.5 km for the intermediate domain, and 1.5 km for the innermost domain [29]. The intermediate and innermost domains are moving nests that follow the TC center anywhere within the outermost domain. Conversely, the outermost domain does not move throughout the forecast period and is roughly centered on the initial TC position (e.g., Figure 1). HWRF is configured with 75 hybrid pressure-sigma vertical levels and a model top of 10 hPa for the North Atlantic basin.
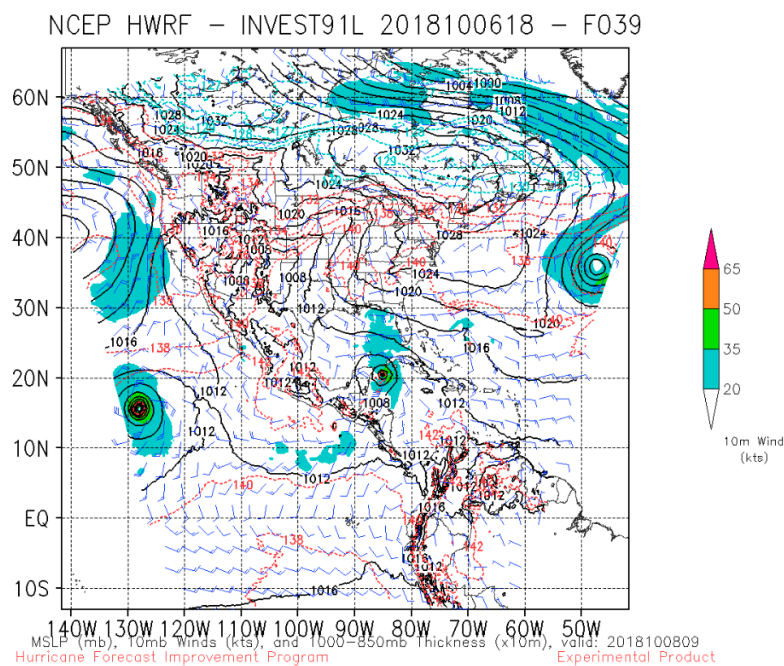

Figure 1. The outermost domain for a Hurricane Weather Research and Forecasting (HWRF) forecast of Hurricane Michael initialized at 1800 UTC on 06 October 2018. (courtesy of EMC).

HWRF is configured with an advanced physics suite that has been extensively tested for TC forecasts [29]. HWRF physics options include the scale-aware simplified Arakawa–

Schubert (SASAS) cumulus parameterization for deep and shallow convection, the Ferrier–Aligo cloud microphysical parameterization for explicit moist physics, the Geophysical Fluid Dynamics Laboratory (GFDL) surface-layer parameterization to account for air–sea interaction over warm water and under high-wind conditions, the Noah land surface model, the rapid radiative transfer model for global circulation models (RRTMG) shortwave and longwave radiation scheme, and the hybrid eddy-diffusivity mass-flux (Hybrid EDMF) planetary boundary layer scheme [29].

3.2. Model Simulations, Verification, and Analysis

The initial conditions and lateral boundary conditions are from the GFS forecast. The forecasts for hurricanes Irma and Michael were initialized at 1200 UTC on 30 August 2017 and 1800 UTC on 06 October 2018, respectively. The forecast periods for each TC were carefully chosen to include the respective RI events and subsequent evolution. The HWRF large-scale environment was compared with the NCEP Global Data Assimilation System/Final 0.25 Degree Global Tropospheric Analyses and Forecast Grids (FNL) to evaluate environmental shear, sea surface temperatures, and mid-level moisture [30]. The advanced diagnostic postprocessing, analysis, and display system (DIAPOST) were used to perform two coordinate transformations, i.e., (1) to convert the model output from the native HWRF E-grid to an A-grid and (2) to interpolate the model output to cylindrical polar coordinates with height and radius in units of km. The transformed variables were used for analyzing the momentum budgets.

3.3. Tangential Wind Momentum Budget Terms

To understand the impact of VWS on the evolution of a TC vortex better, the tangential wind momentum budget is computed, an approach similar to that described in [18,19,31–33]. Equation (1) shows the azimuthally averaged tangential wind momentum budget as follows:

$$\frac{\partial \langle v \rangle}{\partial t} = -<u><f+\zeta> \quad -<w>\frac{\partial \langle v \rangle}{\partial z} \quad -<u'\zeta'> \quad -<w'\frac{\partial v'}{\partial z}> \quad +<D_V>+<D_H> \tag{1}$$

The budget terms are color coded to simplify the identification of each term. In cylindrical coordinates, u, v, and w represent the radial, tangential, and vertical components of velocity, respectively. The vertical component of relative vorticity is denoted by ζ and f is the Coriolis parameter. The azimuthal mean is denoted by < > and eddy (e.g., departure from the azimuthal mean) is denoted by ′ (prime). The highlighted terms on the right-hand side of the (1) are the mean radial influx of absolute vertical vorticity (first term, yellow), the mean vertical advection of mean tangential momentum (second term, blue), the eddy radial vorticity flux (third term, red), the eddy vertical advection of eddy tangential momentum (fourth term, green), and the mean tendency terms due to vertical and horizontal diffusion (fifth term, purple).

The residual term, which includes numerical errors and the pressure gradient, is neglected. The residual may originate from interpolation between the model coordinate system to the polar cylindrical coordinates. This approximation is especially valid for this study because the diffusion tendency terms were explicitly computed within the model and are not included in the residual. We used the outputs from the innermost (1.5 km) domain for our analysis of the vortex spin-up mechanism in terms of (1) in the following section. For both cases, the mean TC motion was removed to calculate the tangential wind momentum budget.

4. Results

4.1. Model Verification: Track and Intensity

Simulated track and intensity produced by HWRF for both TCs are compared with the National Hurricane Center (NHC) best track [34]. Irma's simulated track followed generally close to the best track, except with a slower translation speed (Figure 2a). Michael's simulated track was also quite close to the best track, except for a slight west bias (Figure 2b). The differences between simulated and best tracks in both cases could be due to minor discrepancies in the synoptic-scale environment and will be investigated in later sections. The intensity predictions, as depicted by the evolution of minimum mean sea-level pressure (MSLP) and maximum 10 m winds, are also reasonably reproduced by the model (Figure 3a–d). An RI phase was clearly captured by the simulation of each TC. In the case of Irma (Figure 3a,b), the RI phase is followed by a steady-state phase and then a slow intensification phase. The stages of intensity change are consistent with the descriptions provided in Figure 2a. Hurricane Michael intensified until landfall (Figure 2b). Although predicted values of minimum MSLP were too high and maximum 10 m winds were too weak in the Michael simulation (Figure 3c,d), the hurricane correctly intensified until landfall.
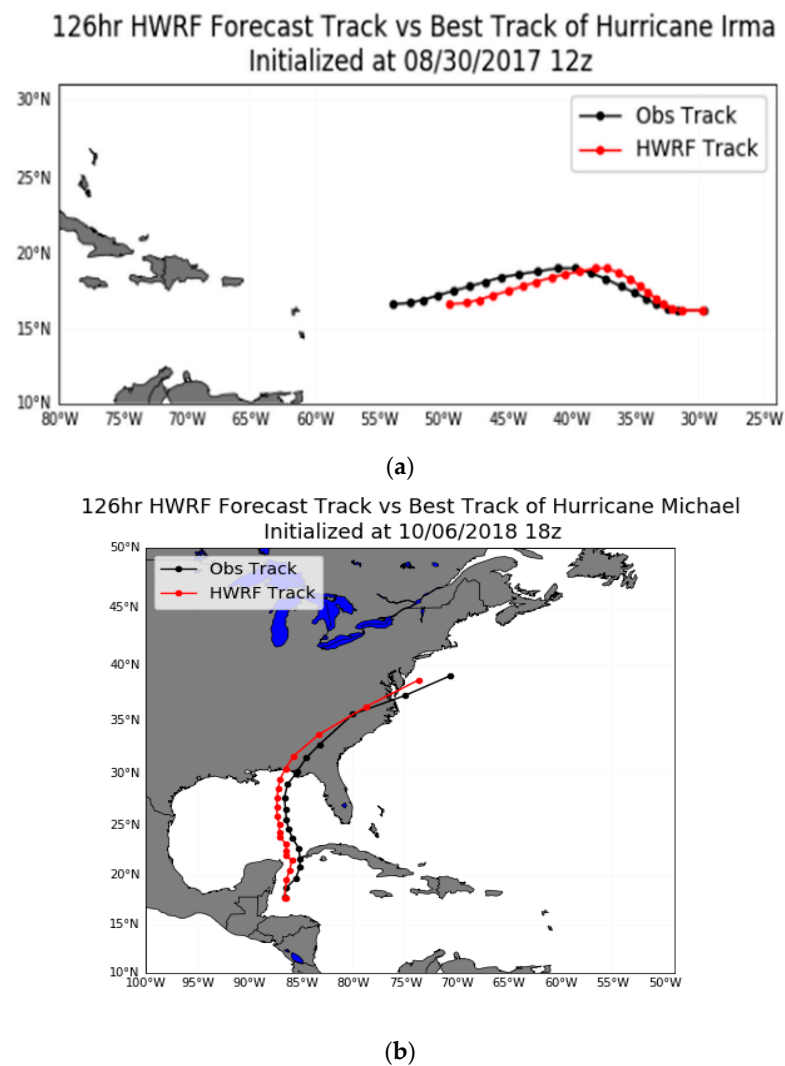

(**a**)

(**b**)

Figure 2. The 126 h HWRF forecast tracks (red) and corresponding observed National Hurricane Center (NHC) best track (black) for (**a**) Hurricane Irma initialized at 1200 UTC on 30 August 2017 and (**b**) Hurricane Michael initialized at 1800 UTC on 06 October 2018. Markers represent the tropical cyclone (TC) position every 6 h.
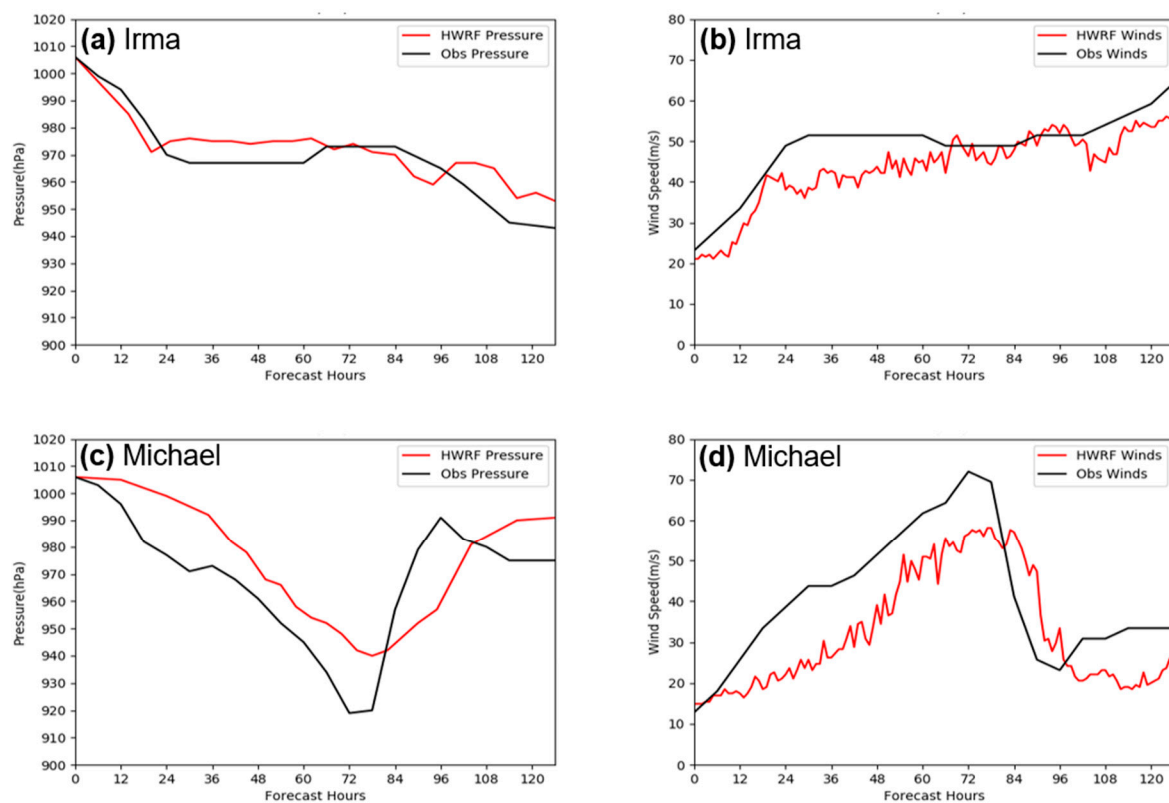
Figure 3. HWRF forecasts (red) are compared with the NHC best track (black) for Hurricane Irma (**a**,**b**) and Hurricane Michael (**c**,**d**). The presented features include (**a**,**c**) minimum mean sea level pressure (hPa) and (**b**,**d**) maximum 10 m winds (m s^{-1}). The forecasts for Hurricane Irma and Hurricane Michael were initialized at 1200 UTC on 30 August 2017 and 1800 UTC on 06 October 2018, respectively.

4.2. Large-Scale Environment

An evaluation of the large-scale (i.e., synoptic-scale) environment is performed for Hurricanes Irma and Michael to assess the fidelity of the HWRF simulations with respect to the GFS analysis (FNL) and to understand environmental forcing on the TC vortices, including the evolution of the tangential wind momentum budget (see Section 4.4). Specifically, this evaluation focuses on the large-scale momentum (e.g., VWS), moisture, MSLP, and sea surface temperatures (SSTs) to identify key differences in the environmental forcing on Hurricane Irma and Hurricane Michael. Irma was embedded in an environment conducive for RI with weak VWS, a moist middle troposphere, and warm SSTs. On the other hand, the environment around Michael was more hostile and generally unsupportive of RI due to strong VWS, although the middle troposphere was moist and SSTs were warm.

Deep-layer VWS is calculated as the 200 hPa wind minus the 850 hPa wind and is typically inversely related to TC intensity change. In other words, TC intensity change tends to be positive (negative) when VWS is weak (strong). Deep-layer VWS and 200 hPa streamlines revealed an environment around Hurricane Irma that was conducive for RI, as shown in HWRF and FNL (Figure 4). In fact, the HWRF and FNL fields are nearly identical at 0000 UTC on 31 August 2017, which is not surprising given that the valid time is only 12 h into the HWRF simulation. Irma was embedded in a zonal strip of VWS less than 15 m s^{-1} that extended from the west coast of Africa to the Lesser Antilles. Higher VWS magnitudes to the north and south of Irma in conjunction with the 200 hPa streamline pattern indicate well-established upper-tropospheric outflow associated with the TC. The outflow to the north of Irma was aided by an upper-tropospheric trough centered at 35° N, 25° W. That trough was not close enough to Irma to force higher VWS values in its inner core. As expected, Irma experienced RI in this low-shear environment as it moved generally

westward (see Figures 2a and 3b), with the onset of the RI period occurring at the time shown in Figure 4. The RI period halted at 1200 UTC on 31 August 2017 (forecast hour 24) as Irma approached a different upper-tropospheric trough to its northwest with VWS greater than 25 m s^{-1}. As shown in Figure 2a, Irma actually turned to the northwest as it approached the trough, which likely contributed to steady-state intensity for the next 36 h after the RI period concluded.
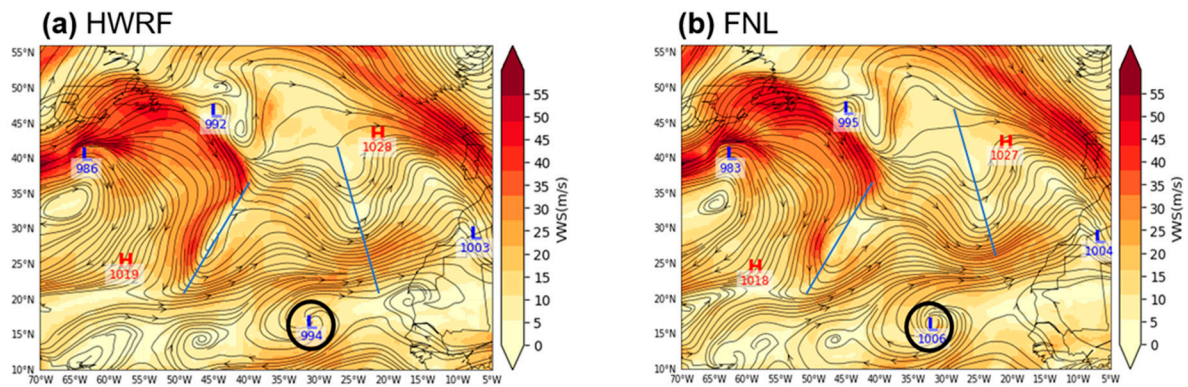

Figure 4. Deep-layer (200–850 hPa) vertical wind shear (VWS, shaded), 200 hPa streamlines, and mean sea level pressure (MSLP) centers in the environment near Hurricane Irma (2017) from (**a**) 12 h into an HWRF forecast initialized at 1200 UTC on 30 August 2017 and (**b**) Final Analysis (FNL) valid at 0000 UTC on 31 August 2017. The center position of Irma is identified by a black circle. VWS has units of m s^{-1}, and MSLP has units of hPa. The trough axes relevant to these discussions are marked by blue lines.

Mid-tropospheric moisture is calculated as the mass-weighted average of relative humidity (RH) in the 700–400-hPa layer and is typically directly proportional to TC intensity change [35–38]. Moist environments support deep convection and thus intensification. HWRF and FNL were, once again, nearly identical, providing more confidence that HWRF reasonably reproduced the large-scale environment near Irma (Figure 5). During the RI period, Irma was associated with a very moist middle troposphere that had RH greater than 80% (Figure 5). In particular, high RH values were noticeable to the north and south of Irma in both HWRF and FNL. A large area of dry air was observed to the northwest of Irma in association with the Saharan air layer, which generally acts to suppress TC intensification. When dry air is entrained into a TC's inner core, it often interrupts the RI process by limiting the amount of moisture necessary to support deep convection [35–38]. Although this dry air did not prevent Irma's RI, it likely played a role in halting the RI process as RH less than 50% began to wrap into the western side of the TC.

Historically, SST has been long known to limit or enhance TC formation and intensification [2,8,11,38]. TCs typically do not develop or intensify over regions with SSTs cooler than 26 °C. As SSTs increase above 26 °C, they drive a larger disequilibrium between the ocean and the atmosphere. As a result, enthalpy fluxes increase to fuel stronger TCs, which, in turn, drive even higher enthalpy fluxes related to increased surface winds. While details of the coupled HWRF simulation on the ocean response to the hurricanes are out of the scope of the current study, a large-scale analysis is carried out in this section to understand the differences between the oceanic environment in the two cases of Hurricanes Irma and Michael.

The HWRF and FNL fields were quite similar, with only minor differences up to 0.5 °C in the environment near Irma (Figure 6). Irma was centered over SSTs near 28 °C, which is warm enough to support deep convection and RI. The MSLP field revealed a weakness in the subtropical ridge to the north of Irma due to a pair of mid-latitude cyclones over the northern North Atlantic (Figures 5 and 6). The TC had been steered generally westward up to this point by the subtropical ridge (Figures 5 and 6). However, the erosion of the subtropical ridge allowed Irma to turn to the northwest, and the TC moved over cooler

waters with SSTs less than 27 °C. Cooler SSTs combined with dry mid-tropospheric air played a significant role in halting the RI process by 1200 UTC on 31 August 2017.
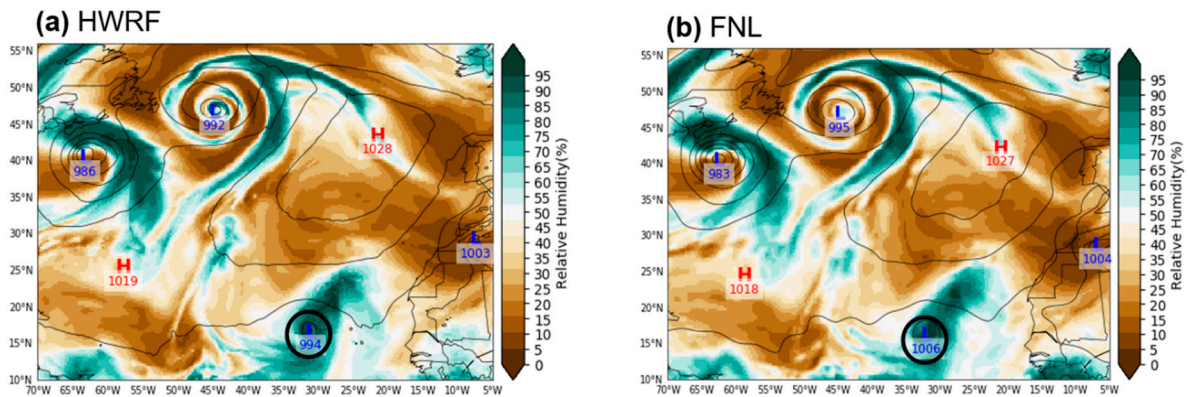

Figure 5. Mid-tropospheric (400–700 hPa average) relative humidity (RH, shaded) and mean sea level pressure (MSLP, contours and centers) in the environment near Hurricane Irma from (**a**) 12 h into an HWRF forecast initialized at 1200 UTC on 30 August 2017 and (**b**) FNL valid at 0000 UTC on 31 August 2017. The center position of Irma is identified by a black circle. RH is measured as a percentage, and MSLP has units of hPa.
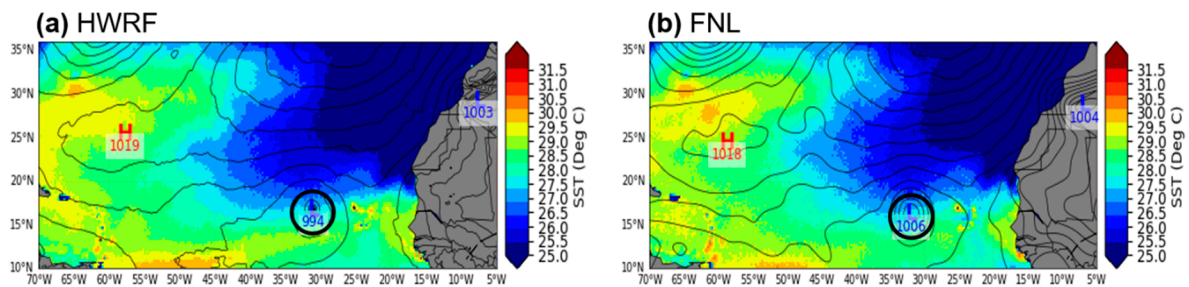

Figure 6. Sea surface temperatures (SSTs, shaded) and mean sea level pressure (MSLP, contours and centers) in the environment near Hurricane Irma from (**a**) 12 h into an HWRF forecast initialized at 1200 UTC on 30 August 2017 and (**b**) FNL valid at 0000 UTC on 31 August 2017. The center position of Irma is identified by a black circle. SST has units of °C, and MSLP has units of hPa.

Contrary to the Irma case, deep-layer VWS and 200 hPa streamlines indicated a hostile environment around Hurricane Michael that was unconducive for RI (Figure 7). Nevertheless, Michael experienced RI for much of its life cycle prior to landfall. Overall, the HWRF and FNL fields were similar at 1800 UTC on 08 October 2018 (forecast hour 48), with only minor differences near Michael. As Michael moved northward (see Figure 2b), it moved into a region of strong VWS (>20 m s^{-1}) that was enhanced by an upper-tropospheric trough positioned over the northern Gulf of Mexico and the United States. An additional upper-tropospheric trough centered to the east of Florida enhanced the outflow on the eastern side of Michael's circulation. The 200 hPa streamlines revealed that upper-tropospheric outflow was well-established to the east of Michael and was virtually non-existent to the west of Michael. This enhanced outflow, albeit asymmetric, became a critical driver of strong deep convection by evacuating mass from the TC circulation in spite of the unfavorable VWS. In essence, the two upper-tropospheric troughs had opposing positive and negative impacts on Michael. As the trough over the United States weakened and moved northward, outflow became more pronounced on the northern and eastern side of Michael's circulation, including a clear northerly outflow channel in the 200 hPa flow to the east of the TC. These outflow channels are known to foster TC intensification by ventilating outflow in a single, narrow pathway [35].
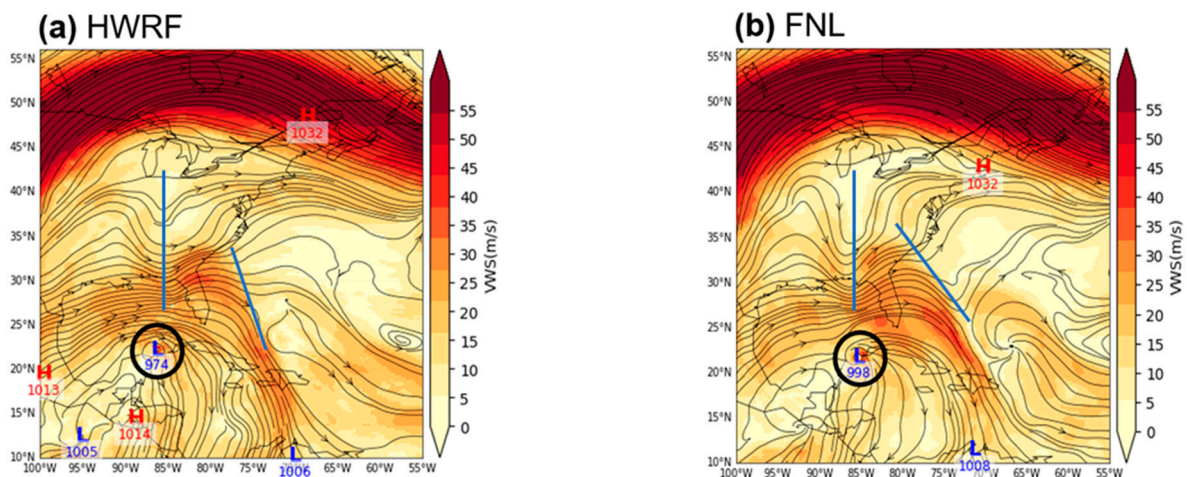
Figure 7. Deep-layer (200–850 hPa) vertical wind shear (VWS, shaded), 200 hPa streamlines, and mean sea level pressure (MSLP) centers in the environment near Hurricane Michael from (**a**) 48 h into an HWRF forecast initialized at 1800 UTC on 06 October 2018 and (**b**) FNL valid at 1800 UTC on 08 October 2018. The center position of Michael is identified by a black circle. VWS has units of m s^{-1}, and MSLP has units of hPa. The trough axes relevant to these discussions are marked by blue lines.

Mid-tropospheric moisture was asymmetric around Hurricane Michael, with RH greater than 80% to the north and east of the TC and a region of drier air (RH < 50%) to the south of the TC (Figure 8). The dry air had clearly intruded into the TC circulation by this time, and dry air near a TC center has the potential to inhibit deep convection, especially when VWS is strong. Overall, the moisture pattern was simulated realistically by HWRF.
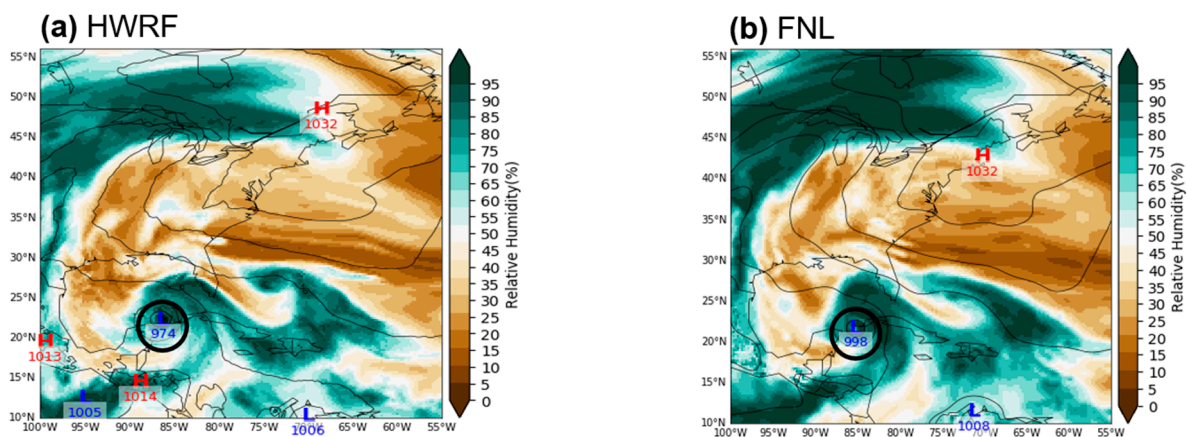

Figure 8. Mid-tropospheric (400–700 hPa average) relative humidity (RH, shaded) and mean sea level pressure (MSLP, contours and centers) in the environment near Hurricane Michael from (**a**) 48 h into an HWRF forecast initialized at 1800 UTC on 06 October 2018 and (**b**) FNL valid at 1800 UTC on 08 October 2018. The center position of Michael is identified by a black circle. RH is measured as a percentage, and MSLP has units of hPa.

Unlike the VWS and moisture fields, very warm SSTs (>29 °C) were supportive of deep convection and RI (Figure 9). While strong VWS likely acted to ventilate Michael's inner core, allowing drier mid-tropospheric air to reach the center of the TC, SSTs may have played a significant role in the intensification process by supplying warm, humid air to the troposphere that could counteract the hostile dry air and shear. It should be mentioned that SSTs in the HWRF simulation (Figure 9a) were 0.5–2 °C cooler than in the analysis (FNL) near Hurricane Michael (Figure 9b). Despite cooler SSTs in HWRF, they were adequately warm to support deep convection and RI (>28 °C). However, these

reduced SSTs in HWRF may have limited the predicted intensification rate, compared to the best track (see Figure 3c,d).
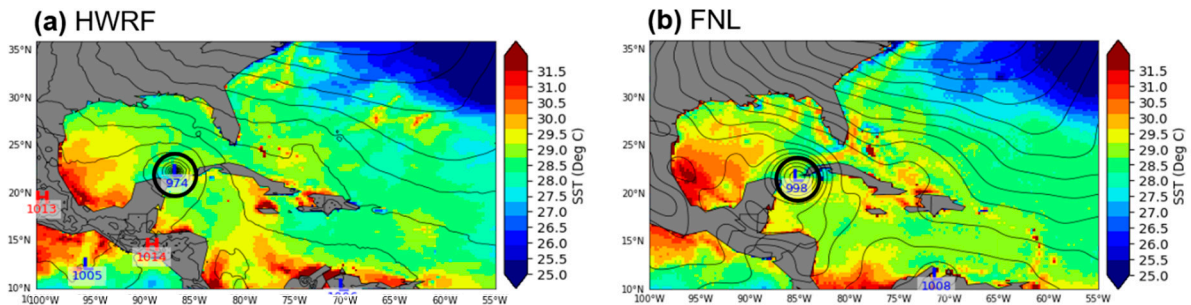

Figure 9. Sea surface temperatures (SSTs, shaded) and mean sea level pressure (MSLP, contours and centers) in the environment near Hurricane Irma from (**a**) 12 h into an HWRF forecast initialized at 1800 UTC on 06 October 2018 and (**b**) FNL valid at 1800 UTC on 08 October 2018. The center position of Michael is identified by a black circle. SST has units of °C, and MSLP has units of hPa.

4.3. TC Inner Core

Latent heating due to convection in the eyewall region of a TC drives the intensification and maintenance of the system. The organization of convection both in the azimuthal and radial directions and eddy processes, especially those associated with the segregation and merging of vortical hot convective clouds, are known to influence TC intensity changes [14,18,19,31,32,39–45]. Therefore, it is critical to understand the organization of convection in order to examine the vortex spin-up mechanism in both TCs. The organization of convection and associated asymmetries are explored in vertical velocity and relative vorticity fields in the upper troposphere (10 km) during RI periods of both TCs (Figures 10 and 11). It is noted that vorticity is scaled by h^{-1} for the convenience of budget calculations (Section 4.4).
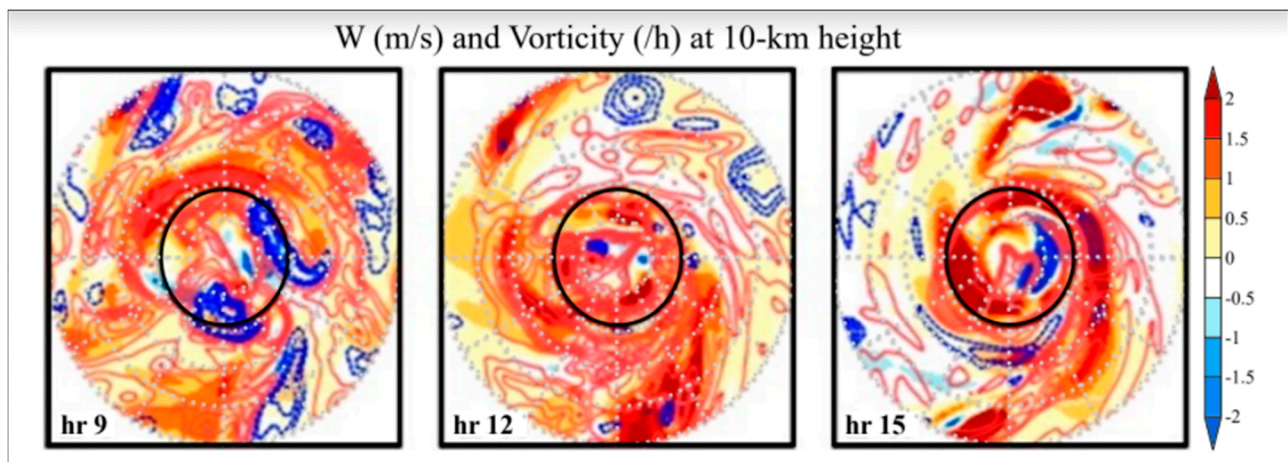

Figure 10. Azimuthal structure of vertical velocity (units of m s^{-1}, shaded) and relative vorticity (units of h^{-1}, contours) at 10 km height during the RI of Hurricane Irma. In all panels, red contours/shades denote positive values, and blue contours/shades denote negative values. The contour interval is 1.0 h^{-1}. The black ring indicates the approximate radius of maximum surface wind. Each box is 200 km × 200 km, with dashed gray range rings every 50 km.
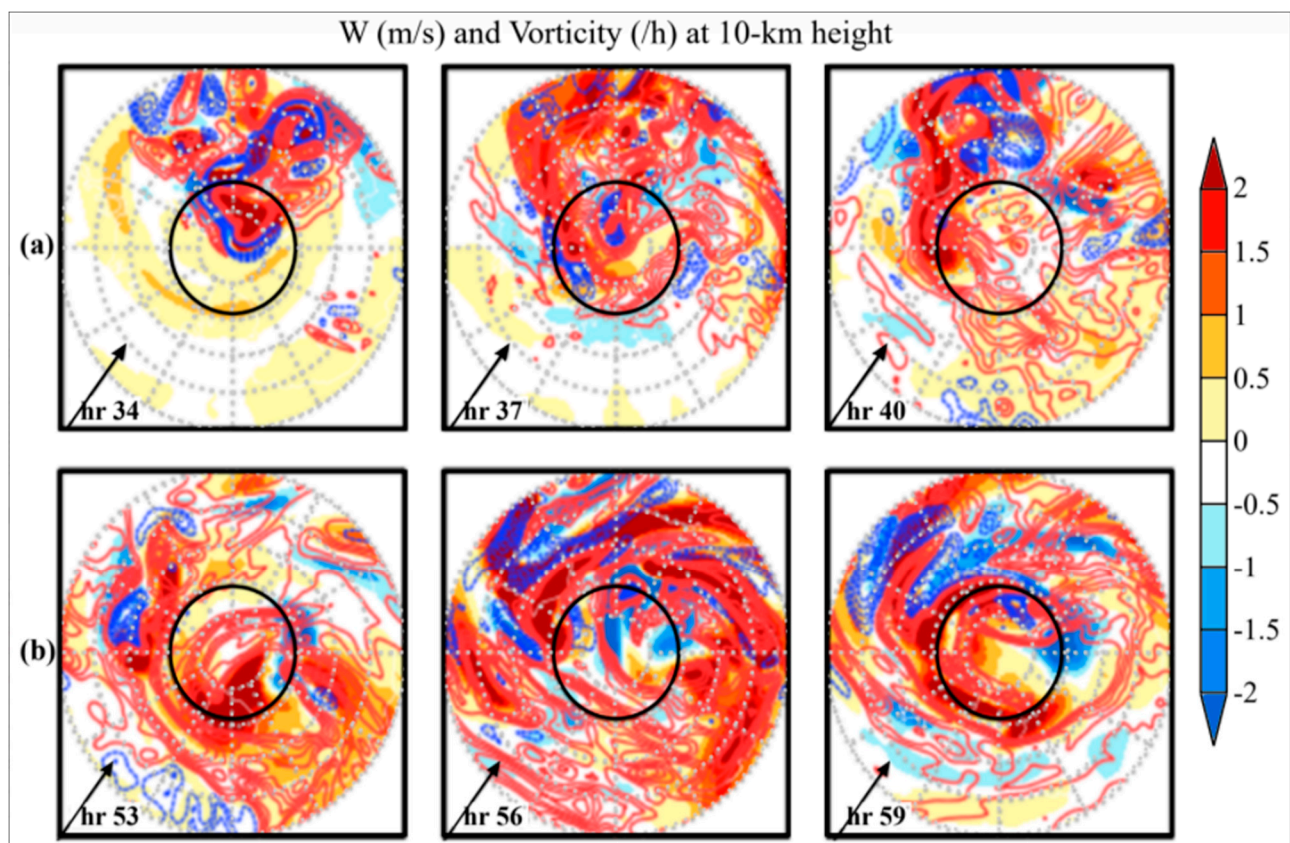
Figure 11. Azimuthal structure of vertical velocity (units of m s^{-1}, shaded) and relative vorticity (units of h^{-1}, contours) at 10 km height during the (**a**) early and (**b**) late RI period of Hurricane Michael. In all panels, red contours/shades denote positive values, and blue contours/shades denote negative values. The contour interval is 1.0 h^{-1}. The black ring indicates the approximate radius of maximum surface wind. Each box is 200 km × 200 km, with dashed gray range rings every 50 km. The arrow shows the approximate direction of deep-layer vertical wind shear.

Figure 10 shows the presence of localized, rotating, deep-convective plumes, so-called vortical hot towers [39,40,44,45], aggregating into mesoscale convective complexes in the horizontal direction (red contours) at a height of 10 km during the RI period of Irma (centered around 12 h). These complexes grew almost symmetrically in both axial and radial directions in the cyclonic, vorticity-rich environment around Irma. On average, the plumes enhance the mean vorticity of the environment (note the abundance of red contours in Figure 10). At 9 h, positive (red contours) and negative (blue contours) vorticity couplets are clearly visible rotating around the TC center. In the TC inner core, these couplets usually develop early in the intensification stage and straddle either side of the local wind maxima in the mesoscale circulation. The negative part of the couplet is usually expelled from the incipient vortex or mixed with an environment of abundant positive vorticity. Additionally, the negative relative vorticity regions are less than or equal to −1.0 h^{-1} and coincident with planetary vorticity that is on the order of 0.2 h^{-1}, indicating that absolute vorticity is negative in these regions and that inertial instability also accounts for the breakup of negative relative vorticity. On the other hand, the positive part of the couplet increases the ambient lower-tropospheric relative vorticity in the region and therefore serves to precondition a strong mean spin up [39]. It should be noted that mixing of negative vorticity in a region rich with positive vorticity may cause some spin down, but frequent convective bursts typically offset those minor negative effects. Indeed, by 12 h and within the TC inner core (i.e., radius < 50 km), the initially dipolar structure of vorticity (red and blue contours) had reorganized into a monopolar, positive vorticity structure (mostly red contours within the black ring) that is accompanied by segregation,

merging and axisymmetrization, as described in [19]. By 15 h, the axisymmetrization process was completed, as indicated by stronger positive vertical velocity (red shade) in the eyewall region with a pronounced monopolar structure. The subsiding motion was observed within the developing eye (blue shade), providing more evidence that Irma had become extremely well organized in the upper troposphere.

In the case of Michael, strong VWS had a significant impact on the organization of convection (Figure 11). Figure 11a shows the vertical motion and vorticity early in the RI period of Michael. Although the vortical convective plumes were organized in the form of mesoscale convective complexes [19] at 34 h, as seen in Irma, merging and segregating of these plumes were restricted mostly downshear and to the left of the shear vector (e.g., northern region). There is also evidence of vorticity couplets, including a long filament of negative vorticity that extended over the TC surface center at this time. As was the case with Irma, negative relative vorticity is of the opposite sign and larger magnitude than the planetary vorticity, indicating that inertial instability is present to assist in the expulsion of these negative vorticity regions.

Nevertheless, even at 10 km height, weak upward motion (shaded in yellow) is present in most of the domain at this time (Figure 11a), perhaps an indication of the larger cyclonic gyre (vorticity-rich environment) that encompassed the circulation of Michael (Section 2b). Later in the early RI stage (37 h), positive vorticity increased in coverage within 50 km of the TC center, consistent with deep convection near or inside of the radius of maximum surface wind, and was prominent in the northern and eastern quadrants of the TC circulation, consistent with a downshear vortex tilt (Figure 11a). However, deep convection and positive vorticity were still weak or absent in the southern and western quadrants of the TC (Figure 11a). Positive vorticity and upward motion continued to increase in coverage to the west and south of the TC center by 40 h (Figure 11a). Despite continued segregation, merging, and mixing in the eyewall region (blue and red contours), the vortical plumes (red contours) contributed to an increase in the mean vorticity of the environment accompanied by stronger upward motion (red shading).

The vortical plumes, drawn into long mesoscale convective structures (red contours), were observed to wrap around the vortex later in the RI period (Figure 11b). These structures, also known as mesocyclones, were reported to have formed in the eyewall region of Hurricane Michael and led to an increase of positive vorticity in all quadrants of the storm (Figure 11b). These mesocyclones could rapidly contribute to the increase in the mean vorticity of the environment and could have helped to sustain the RI of Michael. Furthermore, strong updrafts were also observed on the upshear side of the TC near and within the radius of maximum wind, an ingredient for RI (e.g., [46]). By 59 h, upward motion and positive vorticity had increased in the hurricane's organization, although the structure was not quite monopolar, as in Irma. In fact, vertical velocity exhibited a wavenumber one pattern around the TC center.

Downward motion (e.g., subsidence, downdrafts) was visible at this time within the northern semicircle of the eyewall, as Michael's maximum wind speed at the surface was greater than 45 m s^{-1} (see Figure 3d). This downward motion was also observed in previous studies [47–49], although the positioning of these downdrafts was typically upshear at lower levels. Additionally, negative vorticity (blue contours) was not efficiently mixed out of the circulation, even with the aid of inertial instability, likely due to persistent VWS, indicating eddy spin down that was competing with strong mean spin-up of the vortex throughout the RI period (Figure 11). Interestingly and similar to Irma (Figure 10), other studies [22,41,45], including our earlier ones [7,18,19], have generally observed the near disappearance of negative vorticity near the eyewall region at the end of the merging and axisymmetrization phase. Despite the complicated structure at 10 km height and persistent VWS, localized, rotating, deep-convective plumes [39–45] had propagated to the upshear side of Michael's circulation (i.e., western and southern quadrants), which is an indication that mesoscale convective complexes were growing asymmetrically in the

cyclonic, vorticity-rich environment as the TC intensified (e.g., [19]). Clearly, counteracting processes caused by eddy motions resulting from asymmetric convection cannot be ignored.

4.4. Tangential Wind Momentum Budgets

To understand the influence of asymmetries on the evolution of the mean vortex of Hurricanes Irma and Michael further, we analyzed the tangential momentum budget described in Section 3.3. It should be noted that such a generalized framework may be very useful for understanding both the evolution of symmetric and asymmetric TCs that develop in an environment of high VWS. Our earlier studies [7,18,19] on two other hurricanes, Earl (2010) and Edouard (2014), which developed in environments of significant VWS, indicated that eddy processes had a profound influence on the RI of these storms. Contributions from positive eddy vorticity flux alone were the dominant spin-up mechanism in the case of Earl [18]. An ensemble of forecasts of Edouard showed that eddy terms aided (indicated by red and green in Equation (1)) spin-up in the RI members and impeded intensification of non-intensifying members.

The azimuthally averaged radial wind, tangential wind, and vertical velocity (e.g., Figure 12a–c) is provided to evaluate the TC structure in concert with the budget analysis (e.g., Figure 12d–f). To simplify the following evaluation, the budget terms were combined into mean transport and eddy transport terms. Mean transport terms (e.g., Figure 12d) include the mean radial vorticity flux and the mean vertical advection of mean tangential momentum (i.e., the first two terms on the right-hand side in Equation (1)). Eddy transport terms (e.g., Figure 12e) include the eddy radial vorticity flux, the eddy vertical advection of eddy tangential momentum, and diffusion (i.e., the last four terms on the right-hand side of Equation (1)). It should be noted that the contribution from diffusion (i.e., so-called frictional terms) is restricted to the boundary layer, suggesting that momentum tendencies above 1 km height solely reflect contributions from the eddy terms. Finally, the net tendency of tangential wind momentum is also shown (e.g., Figure 12f) to provide a complete picture of how the budget relates to changes in the TC structure.

At the onset of RI in Hurricane Irma (i.e., 12 h into the HWRF forecast), the radial circulation was represented by a shallow layer of strong inflow roughly 1 km deep in the lower troposphere (Figure 12a). A weak inflow layer developed in the mid-levels (5–9 km) above the primary inflow near the surface. Above the weak second inflow in the upper troposphere was the presence of a moderate outflow of 5 m s^{-1}. At this time, Irma was still a tropical storm with a well-developed deep vortex and maximum winds greater than 25 m s^{-1} within the boundary layer (Figure 12b). The mean vertical motions revealed an updraft core within the eyewall (>1 m s^{-1}), along with some subsidence within the forming eye (Figure 12c).

The corresponding tangential wind momentum budget indicated a net spin-up of the vortex at all heights up to 12 km (Figure 12f). The budget is dominated by the mean transport terms (Figure 12d). These mean terms acted to spin up the vortex throughout the entire depth of the eyewall (compare with Figure 12e) and were strikingly similar to the net tangential wind tendency (compare with Figure 12f). The eddy terms aided spin-up in the lower-to-middle troposphere (up to ~8 km) and spun down the vortex above that (Figure 12e). Eddy-induced spin-down (negative contribution), prominent in the mid-to-upper levels of the TC, was evidence of subsidence within the developing eye that transported lower momentum air downward (Figure 12c). It is also possible that eddy-induced spin-down at these levels was associated with the radially outward eddy vorticity flux. However, the spin-down induced by the eddy terms aloft was not enough to counteract the net spin-up of the vortex. Below 8 km, the eddy vertical advection of eddy tangential wind contributed to vortex spin-up, an indication that rotating, localized updrafts were transporting momentum upward in the eyewall. In the boundary layer, the diffusion terms (Figure 12e) offset the spin-up due to the radial absolute vorticity influx at a distance of 25–60 km from the TC center. The evolution of tangential wind in

Hurricane Irma during its RI period is parallel to findings in previous studies that spin-up of a symmetric TC occurs within the boundary layer and eyewall ([18,50]).
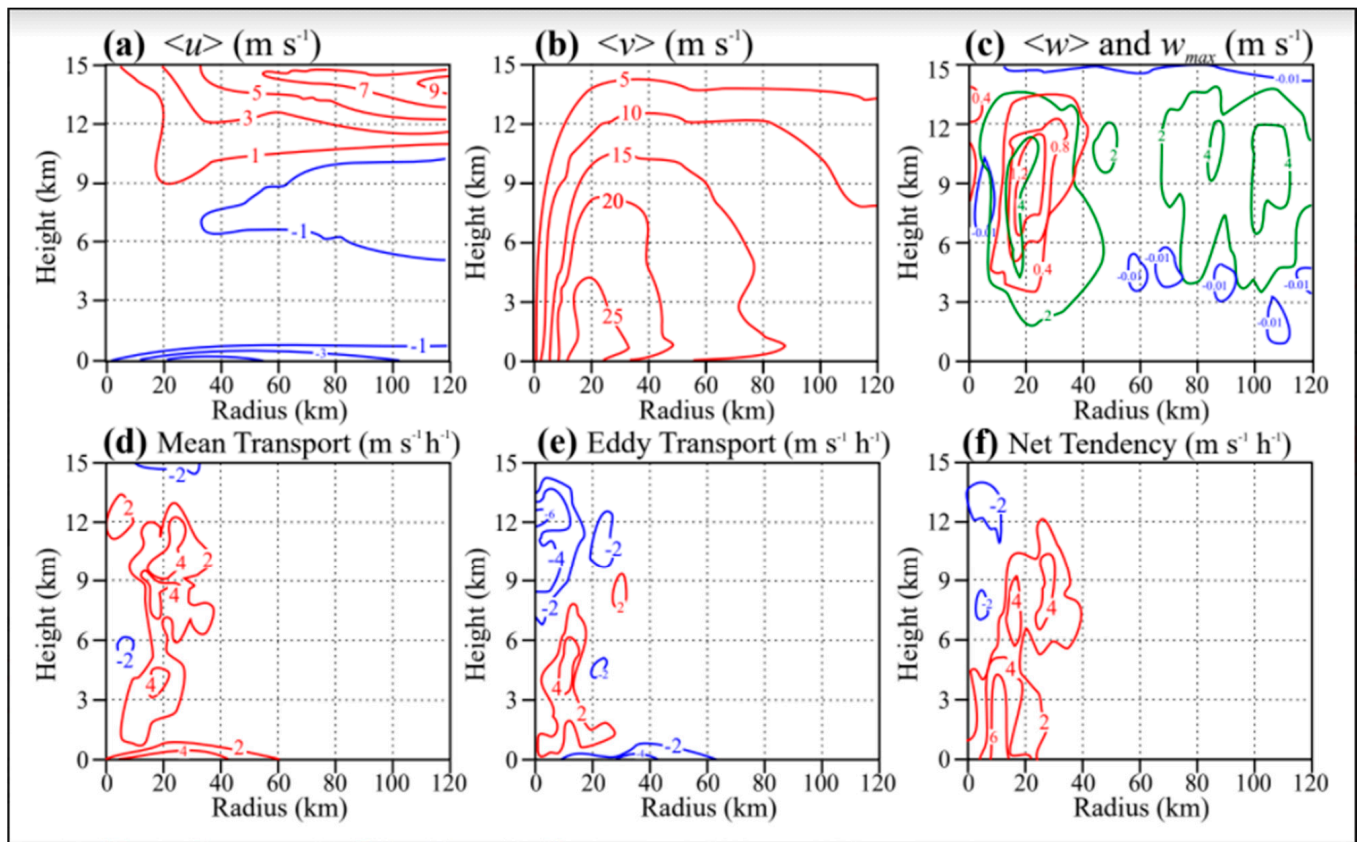

Figure 12. Radius-height momentum (**a**–**c**) and momentum tendency (**d**–**f**) from a 12 h HWRF forecast of Hurricane Irma. Shown: (**a**) radial velocity (contour interval of 2 m s^{-1}); (**b**) tangential velocity (contour interval of 5 m s^{-1}); (**c**) vertical velocity (red contour interval of 0.4 m s^{-1} for positive velocities and blue contour interval of 0.01 m s^{-1} for negative velocities) and maximum vertical velocity (green contour interval of 2 m s^{-1}); (**d**) sum of the mean radial influx of absolute vertical vorticity and the mean vertical advection of the mean tangential momentum (contour interval of 2 m s^{-1} h^{-1}); (**e**) sum of the eddy radial vorticity flux, the eddy vertical advection of eddy tangential momentum, the vertical diffusion, and the horizontal diffusion (contour interval of 2 m s^{-1} h^{-1}); and (**f**) net tangential wind tendency (contour interval of 2 m s^{-1} h^{-1}). All red/blue contours represent positive/negative azimuthally averaged fields. Green contours in (**c**) represent the maximum vertical velocity over all azimuths. All fields are temporally averaged over a 1 h period centered on the forecast hour. The *y*-axis represents height from 0–15 km, and the *x*-axis shows radius from 0–120 km.

Later in the RI period (20 h), Irma had a strong primary inflow roughly 1 km deep in the lower troposphere with weaker inflow above that up to a height of 10 km (Figure 13a). Outflow greater than 7 m s^{-1} was observed above 10 km, indicating a healthy secondary circulation. The mean tangential wind revealed a much stronger TC with maximum surface winds near 40 m s^{-1} and a deep vortex that extended above 16 km (Figure 13b). Figure 13c shows a strong updraft core on the order of 1 m s^{-1} within the eyewall along with strong subsidence within the eye that extended down 6 km height.

The tangential wind momentum budget revealed a net spin-up of the vortex in the eyewall up to ~10 km (Figure 13f), albeit weaker than the spin-up earlier in the RI period (see Figure 12f). The reduced spin-up supports the fact that Irma was close to the end of its RI period. Furthermore, weak spin-down on the inside edge of the eyewall represented a broadening of the eye, another indicator that the end of the RI period was near. The mean transport terms dominated the net tangential wind tendency within the eyewall and hurricane boundary layer (Figure 13d). As expected, frictional terms offset the radial

flux of absolute vorticity in the lowest level of the hurricane boundary layer (Figure 13e). Above the boundary layer, the eddy terms contributed to spin-down in the eyewall region, with strong spin-down in the mid-to-upper levels of the TC (6–12 km height). This eddy-induced spin-down was supported by the transport of lower tangential wind anomalies into regions of higher anomalies, e.g., vertical motions associated with the symmetrization of the vortex throughout the eyewall. These same eddy terms had previously shown a positive contribution to spin-up in the lower troposphere (see Figure 12e).
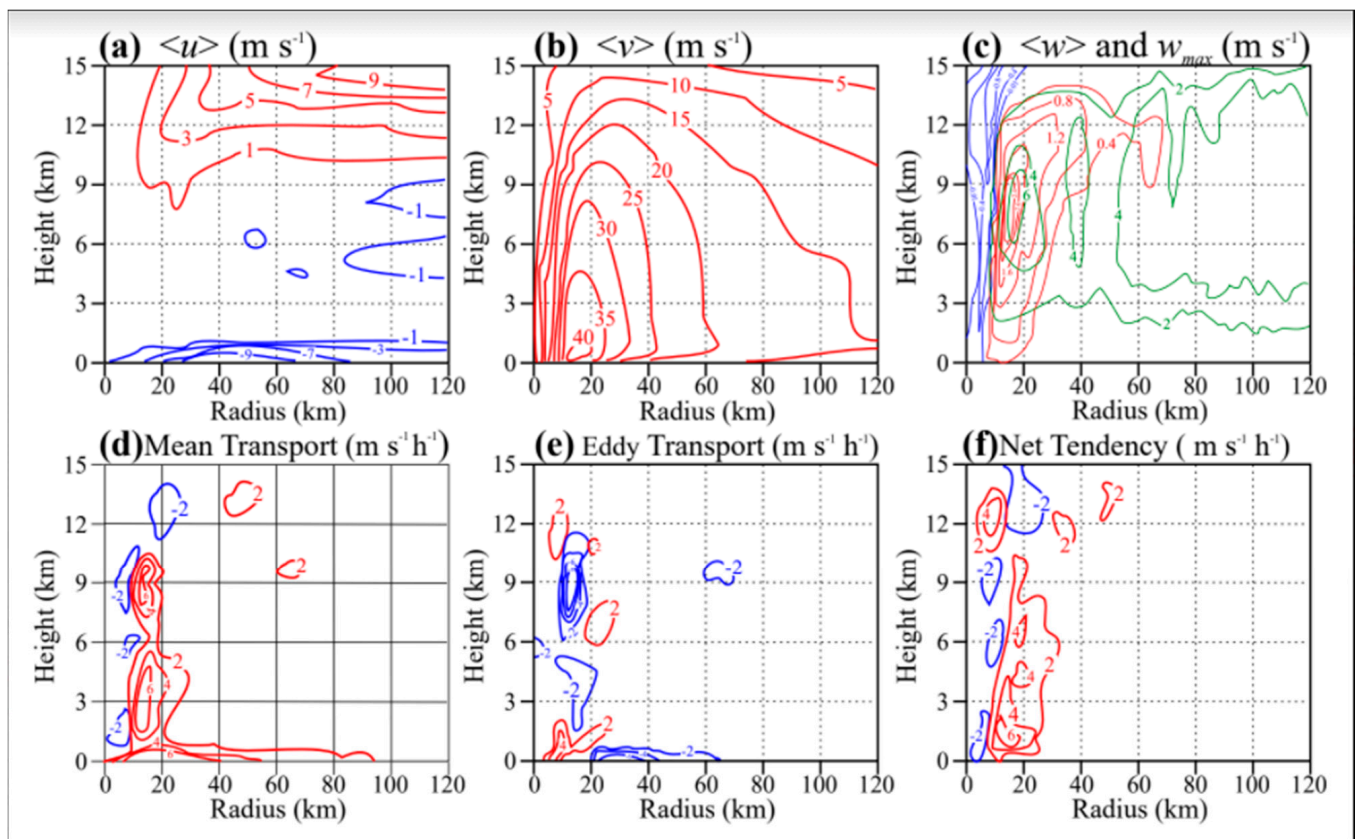

Figure 13. As in Figure 12, except that it shows a 20 h HWRF forecast of Hurricane Irma.

The mean structural evolution of Hurricane Michael during its RI period had similarities and differences with Irma's evolution. Early in the RI period (37 h), Michael was a tropical storm (20–25 m s^{-1}) with weak, deep inflow and asymmetric distribution of vertical velocity (Figure 14a–c). Azimuthally averaged outflow was greater than 7 m s^{-1} aloft and indicated an environment of upper-level divergence despite strong VWS. At this time, Michael was not as well organized as Irma. Although mean vertical motions indicated a weak, unorganized core updraft within the eyewall (Figure 14c), maximum vertical velocities (yellow contours in Figure 14c) provided evidence that strong updrafts within deep convection were occurring within Michael, likely on the downshear (northeast) side of the TC (see Figure 11a).

The tangential wind momentum budget showed a net spin-up of the vortex throughout the troposphere and extending out to 120 km in radius (Figure 14f). Conversely, Irma's spin-up occurred at smaller radii (< 40 km). The eddy transport terms were very important to the net tangential wind tendency, especially below 6 km height and above 11 km height within 30 km of the TC center (Figure 14e). These terms also dominated the net spin up from 6–11 km height at radii larger than 30 km. The mean transport terms weakly contributed to vortex spin-up in the boundary layer and from 6–13 km height (Figure 14d). At lower levels, the vertical advection of mean tangential momentum was near zero due to

weak mean vertical velocity. As expected, the vertical and lateral diffusive terms (frictional terms) negatively contributed to the spin-up process in the hurricane boundary layer and offset spin-up caused by the radial influx of absolute momentum (Figure 14d,e).
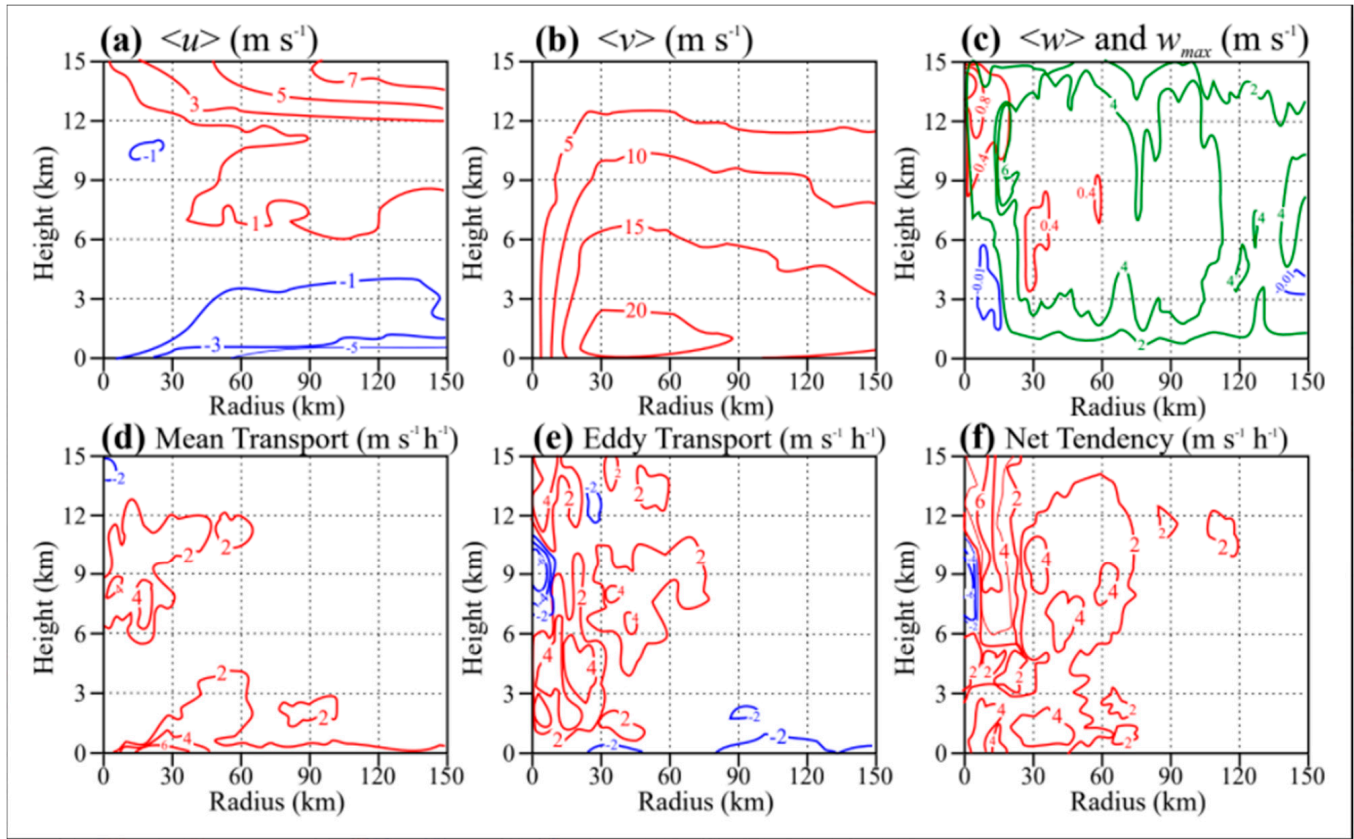

Figure 14. As in Figure 12, except that it shows a 37 h HWRF forecast of Hurricane Michael. The *x*-axis shows the radius from 0–150 km.

Later in the RI period (56 h), Michael's structure had improved considerably, with a strong secondary circulation, a deep vortex with maximum surface winds near 45 m s^{-1}, and a well-organized updraft core (~1 m s^{-1}) that sloped radially outward with height (Figure 15a–c). The secondary circulation consisted of strong inflow near the surface and strong outflow aloft, both greater than 7 m s^{-1} (Figure 15a). Subsidence was observed within the eye at radii less than 20 km (Figure 15c). In the tangential wind momentum budget, the net tangential wind tendency revealed that vortex spin-up was concentrated closer to the now well-defined eyewall (Figure 15f). At this time, the budget was dominated by the mean transport terms within the eyewall and hurricane boundary layer (Figure 15d), consistent with Irma later in its RI period. Furthermore, the eddy transport and diffusive terms partially offset the net vortex spin-up at most levels (Figure 15e), again consistent with Irma later in its RI period (see Figure 13e). Interestingly, the eddy vertical advection of eddy tangential momentum positively contributed to vortex spin-up in some regions, including radially inward of ~10 km and at radii of 20–50 km in a layer from 4–7 km (Figure 15e). Although Michael had symmetrized greatly by this time, the spotty pattern of the eddy transport terms indicates that the TC still had asymmetry because it continued to battle a hostile shear environment, and eddy convective structures were still positively contributing to the spin-up in some regions. Regardless, the tangential wind momentum budget provides evidence that Michael's vortex continued to spin up despite unfavorable VWS.
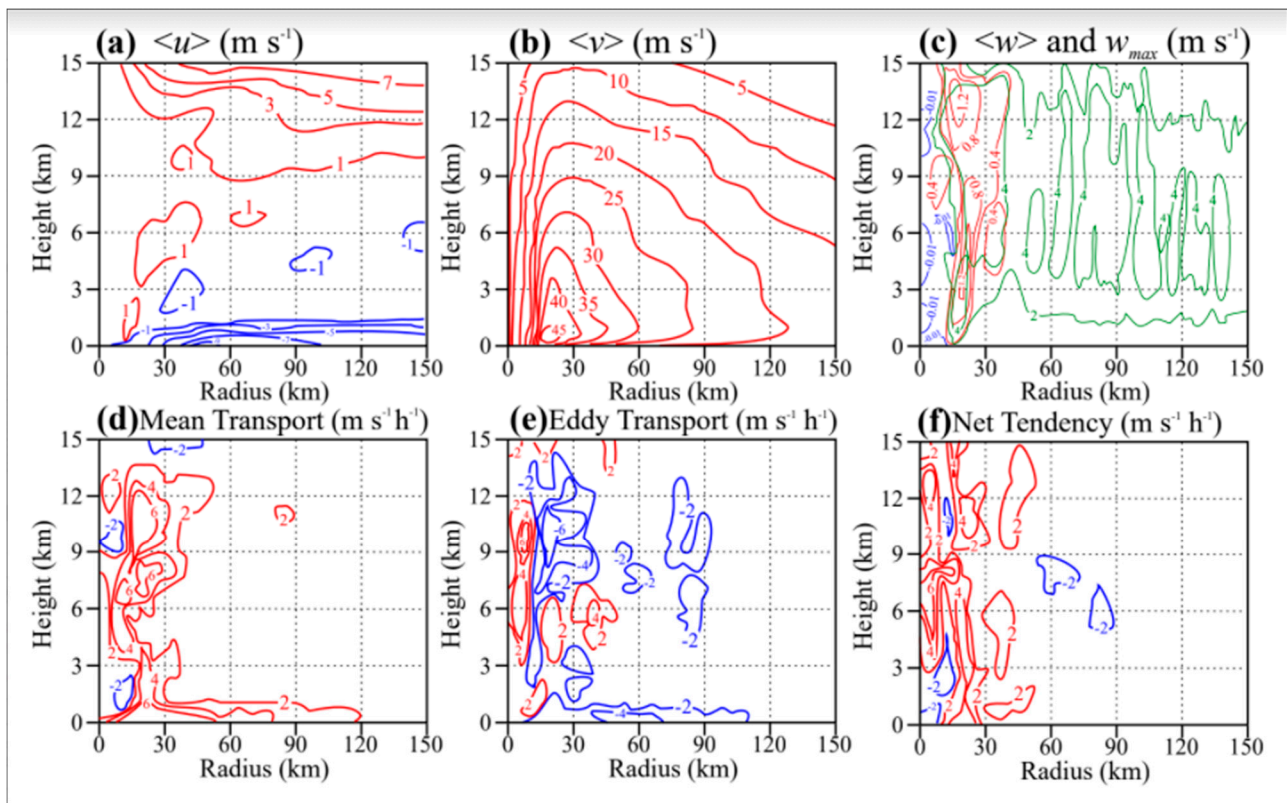
Figure 15. As in Figure 12, except that it shows a 56 h HWRF forecast of Hurricane Michael. The *x*-axis shows the radius from 0–150 km.

5. Discussions and Conclusions

In this study, rapid intensification (RI) was explored in a near axisymmetric TC (Hurricane Irma, 2017) and an asymmetric TC (Hurricane Michael, 2018). Forecasts of Irma and Michael from the HWRF model were analyzed to study how differences in both inner core structure and the large-scale environment were linked to RI. For each TC, the model realistically reproduced the large-scale environment, and its track and intensity. The study aimed to answer the following questions:

(1) How did the environments surrounding Hurricanes Irma and Michael modulate the evolution of TC structure in each case, especially the inner core?
(2) How and why did Hurricane Michael rapidly intensify into a major hurricane despite hostile environmental conditions?
(3) What was the role of eddy and mean transport terms in the intensification processes for Hurricanes Irma and Michael?

Differences in the evolution of environmental VWS were critical to the RI pathways in Irma and Michael. Irma was embedded in an environment of weak VWS (<10 m s^{-1}) that was favorable for RI, while Michael was located in an environment of strong VWS (>10 m s^{-1}), typically unfavorable for RI. Despite these differences in VWS, both TCs experienced RI and became major hurricanes. In Irma, weak VWS allowed for the development of a vertically aligned vortex with deep rotating convective plumes that coalesced into mesoscale clusters in an environment of abundant vorticity (Figure 10). This is consistent with previous studies [19,44], which found that vertical plumes merge and stretch low-level vorticity near the boundary layer to create a stronger inflow that supports intensification. Unlike Irma, strong environmental VWS created a highly asymmetric structure in Michael, with convection primarily located in the downshear left quadrant. Strengthening of the vorticity as it propagated into the upshear left region was observed early in the RI period (Figure 11a). Later in the RI period, an abundance of vorticity near the radius of maximum

winds indicated the merging of the lower- and upper-tropospheric vortices, resulting in a more symmetric structure (Figure 11b).

The initially symmetric structure of Irma and the asymmetric structure of Michael led to key differences in the tangential wind momentum budget. Both early and later in Irma's RI period, the spin-up of tangential winds was dominated by the mean radial transport of absolute vorticity, especially in the boundary layer, and the vertical advection of the mean tangential momentum within the eyewall region (Figures 12d–f and 13d–f). The eddy transport terms (Figure 12e) contributed to the vortex spin-up above the boundary layer up to the middle troposphere. In particular, the eddy vertical advection of eddy tangential wind was responsible for transporting momentum vertically in localized updrafts. At higher altitudes (7–15 km), eddy-induced spin-down represented the development of the eye, where lower tangential wind anomalies were transported downward via subsidence. As expected, diffusion terms counteracted and offset spin-up in the hurricane boundary layer. The overall spin-up process occurred solely in the eyewall. These results are parallel to findings in previous studies that the spin-up of a symmetric TC occurs within the eyewall boundary region [18,19]. Later in the RI period, the mean transport terms continued to dominate the tangential wind tendency in Irma, and the eddy transport terms became negative in the eyewall region, indicating a counteracting of the spin-up induced by the mean terms (Figure 13d–f).

The eddy transport terms become negative due to the vertical advection of lower tangential wind anomalies into regions of higher tangential wind anomalies, thus contributing to a reduction of momentum and a spin-down of the vortex. However, more analysis is required to determine the exact eddy processes that cause vortex spin-down, which will be the topic of future research. This eddy-induced spin-down could be accomplished through anomalous downdrafts (e.g., weaker updrafts), acting upon tangential wind anomalies that increase downward, or through anomalous updrafts (e.g., stronger updrafts), acting upon tangential wind anomalies that increase upward.

Early in Michael's RI period, eddy transport terms contributed more to the net tangential wind spin-up than the mean transport terms, especially from 1–7 km (Figure 14e). Weak spin-up induced by the mean transport terms is explained by the highly asymmetric nature of Michael at this time. For example, although maximum vertical velocity values were greater than 4 m s^{-1}, azimuthal averages of vertical velocity were near zero (Figure 14c). The mean transport terms were much weaker in Michael than in Irma early in their respective RI periods, consistent with previous evaluations of asymmetric TCs [7,18,19]. A novel result is the notion that the eddy transport terms contributed to vortex spin-up at low levels rather than upper levels, which provides evidence that these terms can help initiate RI at low levels within a developing eyewall. These eddy transport terms allowed Michael to overcome unfavorable VWS by transporting higher tangential wind anomalies into regions of lower tangential wind anomalies, presumably through localized convective updrafts that distributed momentum upward in the eyewall. As Michael rapidly intensified, the TC became more symmetric. Consequently, the mean transport terms dominated the net tangential wind spin-up later in the RI period. As in Irma, the eddy transport terms mostly counteracted the vortex spin-up, presumably through similar mechanisms.

We conclude that the pathway to vortex spin-up through positive tangential wind tendency differs for asymmetric (i.e., sheared) and axisymmetric TCs. The former relies on eddy transport terms, especially the eddy vertical advection of eddy tangential momentum, early in the RI period when mean transport is weak. The latter is dominated by mean transport terms, both radial and vertical, with secondary contributions from the eddy transport terms. As an asymmetric TC rapidly intensifies, it typically becomes more symmetric, leading to similar contributions from budget terms later in the RI period, as seen in axisymmetric cases. Future research will focus on a closer inspection of eddy terms to diagnose precisely how symmetrization of the vortex and vertical motions are connected to tangential wind tendency in rapidly intensifying TCs. In particular, we will concentrate

on how eddy transport terms redistribute momentum to enhance vortex spin-up early in RI periods and to counteract vortex spin-up later in RI periods.

References

1. 2019 HFIP R&D Activities Summary: Recent Results and Operational Implementation. HFIP Technical Report: HFIP 2018-1. Available online: http://www.hfip.org/documents/HFIP_AnnualReport_FY2019.pdf (accessed on 13 January 2021).
2. Kaplan, J.; DeMaria, M.; Knaff, J.A. A revised tropical cyclone rapid intensification index for the Atlantic and eastern North Pacific basins. *Weather Forecast.* **2010**, *25*, 220–241. [CrossRef]
3. Willoughby, H.E.; Clos, J.A.; Shoreibah, M.G. Concentric eyewalls, secondary wind maxima, and the evolution of the hurricane vortex. *J. Atmos. Sci.* **1982**, *39*, 395–411. [CrossRef]
4. Kossin, J.; Schubert, W.H. Mesovortices, polygonal flow patterns, and rapid pressure falls in hurricane-like vortices. *J. Atmos. Sci.* **2001**, *58*, 2196–2209. [CrossRef]
5. Eastin, M.D.; Gray, W.M.; Black, P.G. Buoyancy of convective vertical motions in the inner core of intense hurricanes. Part I: General statistics. *Mon. Wea. Rev.* **2005**, *133*, 188–208. [CrossRef]
6. Eastin, M.D.; Gray, W.M.; Black, P.G. Buoyancy of convective vertical motions in the inner core of intense hurricanes. Part II: Case studies. *Mon. Wea. Rev.* **2005**, *133*, 209–227. [CrossRef]
7. Chen, H.; Gopalakrishnan, S. A study on the asymmetric rapid intensification of Hurricane Earl (2010) using the HWRF system. *J. Atmos. Sci.* **2015**, *72*, 531–550. [CrossRef]
8. Kaplan, J.; DeMaria, M. Large scale characteristics of rapidly intensifying tropical cyclones in the North Atlantic basin. *Weather Forecast.* **2003**, *18*, 1093–1108. [CrossRef]
9. Schubert, W.H.; Hack, J.J. Inertial stability and tropical cyclone development. *J. Atmos. Sci.* **1982**, *39*, 1687–1697. [CrossRef]
10. Frank, W.M.; Ritchie, E.A. Effects of vertical wind shear on the intensity and structure of numerically simulated hurricanes. *Mon. Wea. Rev.* **2001**, *129*, 2249–2269. [CrossRef]
11. Kaplan, J.; Rozoff, C.M.; DeMaria, M.; Sampson, C.R.; Kossin, J.P.; Velden, C.S.; Cione, J.J.; Dunion, J.P.; Knaff, J.A.; Zhang, J.A.; et al. Evaluating environmental impacts on tropical cyclone rapid intensification predictability utilizing statistical models. *Weather Forecast.* **2015**, *30*, 1374–1396. [CrossRef]
12. Bhalachandran, S.; Nadimpalli, R.; Osuri, K.K.; Marks, F.D., Jr.; Gopalakrishnan, S.; Subramanian, S.; Mohanty, U.C.; Niyogi, D. On the processes influencing rapid intensity changes of tropical cyclones over the Bay of Bengal. *Sci. Rep.* **2019**, *9*, 3382. [CrossRef]
13. Tang, B.; Emanuel, K. Midlevel ventilation's constraint on tropical cyclone intensity. *J. Atmos. Sci.* **2010**, *67*, 1817–1830. [CrossRef]
14. Riemer, M.; Montgomery, M.T.; Nicholls, M.E. A new paradigm for intensity modification of tropical cyclones: Thermodynamic impact of vertical wind shear on the inflow layer. *Atmos. Chem. Phys.* **2010**, *10*, 3163–3188. [CrossRef]
15. Molinari, J.; Dodge, P.; Vollaro, D.; Corbosiero, K.L.; Marks, F., Jr. Mesoscale aspects of the downshear reformation of a tropical cyclone. *J. Atmos. Sci.* **2006**, *63*, 341–354. [CrossRef]
16. Molinari, J.; Vollaro, D. Rapid intensification of a sheared tropical storm. *Mon. Weather Rev.* **2010**, *138*, 3869–3885. [CrossRef]
17. Rios-Berrios, R.; Torn, R.D.; Davis, C.A. An ensemble approach to investigate tropical cyclone intensification in a sheared environment. Part I: Katia (2011). *J. Atmos. Sci.* **2016**, *73*, 71–93. [CrossRef]
18. Leighton, H.; Gopalakrishnan, S.; Zhang, J.A.; Rogers, R.F.; Zhang, Z.; Tallapragada, V. Azimuthal distribution of deep convection, environmental factors and tropical cyclone rapid intensification: A perspective from HWRF ensemble forecasts of Hurricane Edouard (2014). *J. Atmos. Sci.* **2018**, *75*, 275–295. [CrossRef]

19. Gopalakrishnan, S.; Osuri, K.; Marks, F.; Mohanty, U.C. An inner-core analysis of the axisymmetric and asymmetric intensification of tropical cyclones: Influence of shear. *Mausam* **2019**, *70*, 667–690.
20. Cangialosi, J.P.; Latto, A.S.; Berg, R. National Hurricane Center Tropical Cyclone Report: Hurricane Irma. *Natl. Hurric. Cent.* **2018**, 1–111. Available online: https://www.nhc.noaa.gov/data/tcr/AL112017_Irma.pdf (accessed on 17 January 2021).
21. Bevin, J.L., II; Berg, R.; Hagen, A. National Hurricane Center Tropical Cyclone Report: Hurricane Michael. *Natl. Hurric. Cent.* **2019**, 1–86. Available online: https://www.nhc.noaa.gov/data/tcr/AL142018_Michael.pdf (accessed on 17 January 2021).
22. Gopalakrishnan, S.G.; Marks, F.; Zhang, X.J.; Bao, J.W.; Yeh, K.S.; Atlas, R. The Experimental HWRF System: A Study on the Influence of Horizontal Resolution on the Structure and Intensity Changes in Tropical Cyclones Using an Idealized Framework. *Mon. Weather Rev.* **2011**, *139*, 1762–1784. [CrossRef]
23. Gopalakrishnan, S.G.; Goldenberg, S.; Quirino, T.; Zhang, X.; Marks, F., Jr.; Yeh, K.S.; Atlas, R.; Tallapragada, V. Toward Improving High-Resolution Numerical Hurricane Forecasting: Influence of Model Horizontal Grid Resolution, Initialization and Physics. *Weather Forecast.* **2012**, *27*, 647–666. [CrossRef]
24. Gopalakrishnan, S.G.; Marks, F.D.; Zhang, J.A.; Zhang, X.; Bao, W.J.; Tallapragada, V. A study of the impacts of vertical diffusion on the structure and intensity of the tropical cyclones using the high resolution HWRF system. *J. Atmos. Sci.* **2013**, *70*, 524–541. [CrossRef]
25. Bao, J.-W.; Gopalakrishnan, S.G.; Michelson, S.A.; Marks, F.D.; Montgomery, M.T. Impact of physics representations in the HWRFX on simulated hurricane structure and pressure–wind relationships. *Mon. Weather Rev.* **2012**, *140*, 3278–3299. [CrossRef]
26. Tallapragada, V.; Kieu, C.; Kwon, Y.; Trahan, S.; Liu, Q.; Zhang, Z.; Kwon, I.H. Evaluation of storm structure from the operational HWRF model during 2012 implementation. *Mon. Weather Rev.* **2014**, *142*, 4308–4325. [CrossRef]
27. Atlas, R.; Tallapragada, V.; Gopalakrishnan, S.G. Advances in tropical cyclone intensity forecasts. *Mar. Technol. J.* **2015**, *49*, 149–160. [CrossRef]
28. Janjić, Z.I.; Gerrity, J.P., Jr.; Nickovic, S. An alternative approach to nonhydrostatic modeling. *Mon. Weather Rev.* **2001**, *129*, 1164–1178. [CrossRef]
29. Biswas, M.K.; Abarca, S.; Bernardet, L.; Ginis, I.; Grell, E.; Iacono, M.; Kalina, E.; Liu, B.; Liu, Q.; Marchok, T.; et al. Hurricane Weather Research and Forecasting (HWRF) Model: 2018. *Sci. Doc.* **2018**. Available online: https://dtcenter.org/HurrWRF/users/docs/index.php (accessed on 7 January 2021).
30. National Centers for Environmental Prediction; National Weather Service; NOAA; U.S. Department of Commerce. 2015, Updated Daily. NCEP GDAS/FNL 0.25 Degree Global Tropospheric Analyses and Forecast Grids. Research Data Archive at the National Center for Atmospheric Research, Computational and Information Systems Laboratory. Available online: https://rda.ucar.edu/datasets/ds083.3/ (accessed on 27 January 2021). [CrossRef]
31. Montgomery, M.T.; Kilroy, G.; Smith, R.K.; Črnivec, N. Contribution of mean and eddy momentum processes to tropical cyclone intensification. *Q. J. R. Meteorol. Soc.* **2020**, *146*, 3101–3117. [CrossRef]
32. Persing, J.; Montgomery, M.T.; McWilliams, J.C.; Smith, R.K. Asymmetric and axisymmetric dynamics of tropical cyclones. *Atmos. Chem. Phys.* **2013**, *13*, 12299–12341. [CrossRef]
33. Hendricks, E.A.; Peng, M.S.; Fu, B.; Li, T. Quantifying Environmental Control on Tropical Cyclone Intensity Change. *Mon. Weather Rev.* **2010**, *138*, 3243–3271. [CrossRef]
34. Rappaport, E.N.; Franklin, J.L.; Avila, L.A.; Baig, S.R.; Beven, J.L.; Blake, E.S.; Burr, C.A.; Jiing, J.G.; Juckins, C.A.; Knabb, R.D.; et al. Advances and challenges at the National Hurricane Center. *Weather Forecast.* **2009**, *24*, 395–419. [CrossRef]
35. Wu, L.; Su, H.; Fovell, R.G.; Wang, B.; Shen, J.T.; Kahn, B.H.; Hristova-Veleva, S.M.; Lambrigtsen, B.H.; Fetzer, E.J.; Jiang, J.H. Relationship of environmental relative humidity with North Atlantic tropical cyclone intensity and intensification rate. *Geophys. Res. Lett* **2012**, *39*, L2080. [CrossRef]
36. Tang, B.; Emanuel, K. Sensitivity of tropical cyclone intensity to ventilation in an axisymmetric model. *J. Atmos. Sci.* **2012**, *69*, 2394–2413. [CrossRef]
37. Ge, X.; Li, T.; Peng, M. Effects of Vertical Shears and Midlevel Dry Air on Tropical Cyclone Developments. *J. Atmos. Sci.* **2013**, *70*, 3859–3875. [CrossRef]
38. Tao, D.; Zhang, F. Effect of environmental shear, sea surface temperature, and ambient moisture on the formation and predictability of tropical cyclones: An ensemble mean perspective. *J. Adv. Model. Earth Syst.* **2014**, *6*, 384–404. [CrossRef]
39. Hendricks, E.A.; Montgomery, M.T.; Davis, C.A. The role of "vortical" hot towers in the formation of tropical cyclone Diana (1984). *J. Atmos. Sci.* **2004**, *61*, 1209–1232. [CrossRef]
40. Yang, B.; Wang, Y.Q.; Wang, B. The effect of internally generated inner-core asymmetries on tropical cyclone potential intensity. *J.Atmos.Sci.* **2007**, *64*, 1165–1188. [CrossRef]
41. Smith, R.K.; Montgomery, M.T. Toward clarity on understanding tropical cyclone intensification. *J. Atmos. Sci.* **2015**, *72*, 3020–3031. [CrossRef]
42. Nguyen, S.; Smith, R.; Montgomery, M. Tropical-cyclone intensification and predictability in three dimensions. *Q. J. R. Meteorol. Soc.* **2008**, *134*, 563–582.
43. Zhang, D.L.; Liu, Y.B.; Yau, M.K. A multiscale numerical study of Hurricane Andrew (1992). Part IV: Unbalanced flows. *Mon.Weather Rev.* **2001**, *129*, 92–107. [CrossRef]
44. Montgomery, M.T.; Nicholls, M.E.; Cram, T.A.; Saunders, A.B. A vortical hot tower route to tropical cyclogenesis. *J. Atmos. Sci.* **2006**, *63*, 355–386. [CrossRef]

45. Montgomery, M.T.; Smith, R.K. Paradigms for tropical cyclone intensification. *Aust. Meteorol. Oceanogr. J.* **2014**, *64*, 37–66. [CrossRef]

46. Rogers, R.F.; Reasor, P.D.; Zhang, J.A. Multiscale Structure and Evolution of Hurricane Earl (2010) during Rapid Intensification. *Monthly Weather Review.* **2015**, *143*, 536–562. [CrossRef]

47. Corbosiero, K.L.; Molinari, J. The effects of vertical wind shear on the distribution of convection in tropical cyclones. *Mon. Weather Rev.* **2002**, *130*, 2110–2123. [CrossRef]

48. Corbosiero, K.L.; Molinari, J. The relationship between storm motion, vertical wind shear, and convective asymmetries in tropical cyclones. *J. Atmos. Sci.* **2003**, *60*, 366–376. [CrossRef]

49. Rogers, R.; Reasor, P.; Lorsolo, S. Airborne Doppler observations of the inner-core structural differences between intensifying and steady-state tropical cyclones. *Mon. Weather Rev.* **2013**, *141*, 2970–2991. [CrossRef]

50. Rappin, E.D.; Morgan, M.C.; Tripoli, G.J. The Impact of Outflow Environment on Tropical Cyclone Intensification and Structure. *J. Atmos. Sci.* **2011**, *68*, 177–194. [CrossRef]